Low Frequency Tibial Neuromodulation Increases Voiding Activity - A Computational Model

Aidan McConnell-Trevillion[1,*], Milad Jabbari[1], Abbas Erfanian[2], and Kianoush Nazarpour[1,*]

[1]University of Edinburgh, School of Informatics, Edinburgh, Scotland
[2]Iran University of Science and Technology, Tehran, Iran
[*]Corresponding Author(s): a.mcconnell-trevillion@ed.ac.uk (AMT); kianoush.nazarpour@ed.ac.uk (KN)

ABSTRACT

Despite its clinical adoption, there remains a lack of understanding about how tibial nerve stimulation (TNS) improves lower urinary tract symptoms. Current evidence indicates that TNS ameliorates overactive bladder by the inhibition of micturition related activity in the brainstem and spinal cord. We present a detailed computational model and demonstrate that TNS can also induce excitatory effects via brainstem specific activity, proposing non-invasive neuromodulation as a treatment for urinary retention.

Main Body

Micturition is regulated by a dynamic reflexive process that switches between periods of storing and releasing urine held in the bladder. This cycle is mediated by a complex network of autonomic and somatic neurons across the central and peripheral nervous systems[1,2,3].

Experimental research suggests that the tibial nerve has a significant influence on the function of this system[4,5]. Projections from the tibial nerve to the spine are thought to inhibit afferent sensory neurons[6,7,8] and potentially several midbrain nuclei including the Periaquaductal Grey (PAG) and Pontine Micturition Centre (PMC)[9,10,11] via both classical and opioidergic mechanisms[12]. This differential mechanism of action likely explains the ability of the tibial nerve to inhibit both nociceptive and non-nociceptive bladder activity[13].

While there has been considerable research conducted on the specific targets of tibial nerve projections, and the functional effects of tibial nerve stimulation (TNS) on bladder activity[13], to date the effects of TNS on the micturition control circuit remain understudied. This is particularly relevant given the clinical adoption of TNS as an intervention for the management of lower urinary tract symptoms[13,14].

We sought to produce a detailed computational model of the lower urinary tract and its control system to study the neuromodulatory effects of TNS. We simulated the bladder control network using a modified version of the circuit proposed by De Groat *et al.*[15] (methods). To ensure that the model accurately captured the system level effects of real bladder activity, the parameters and synaptic weights of the simulation were fitted using previously generated experimental rodent data[16], as shown in fig. 1A-B.

As the primary goal of the study was to analyse the circuit level effects of TNS, several modifications were made to the model. These included the simulation of the tibial nerve and its projections, and the use of a simplified representation of the bladder as opposed to a full biophysical simulation, as depicted in fig. 1C and methods. We focused on normal bladder function, hence nociceptive bladder afferents were not included in our model. To simulate the effects of both opioidergic and classical inhibition, neurons and synapses were represented in terms of ionic conductance (methods).

In line with previous research, the tibial nerve was modelled to project to second order afferents via classically inhibitory synapses and both the PMC and PAG via opioidergic connections as shown in fig. 1C. To provide fine control over the level of tibial modulation applied to the system, the firing rate of the neuron and its projections were clamped (methods).

The normal and unmodulated behaviour of the circuit was promising. For a given set of bladder data the model produced activity indicative of ordinary lower urinary tract function. During periods of low bladder pressure, efferent projections associated with urine storage (hypogastric and pudendal) were tonically active, while pelvic projections associated with voiding, were silent. During voiding events, simultaneous activity in the pelvic nerve and inhibition of the hypogastric and pudendal nerves was observed, which aligned with the input data, suggesting that the model mimicked the complex switching behaviours required to mediate lower urinary tract behaviour (see fig. 2A) allowing it to serve as an accurate baseline upon which to test the impact of modulation.

Analysing the effects of TNS on the system revealed an intriguing trend. As expected, high frequency TNS silenced pelvic efferent activity under bladder pressures sufficient to induce urination, suggesting the intervention prevented the circuit from switching to a void-promoting state (see fig. 2B(i)). This observation indicates that the model can effectively simulate typical TNS interventions which utilise 10-20Hz stimulation to enhance bladder capacity[13,14]. In contrast, administering TNS at frequencies lower than 3Hz amplified pelvic nerve activity (see fig. 2B(i)) with 1Hz stimulation driving an average 7.9 fold increase (± 1.1) in pelvic output. This stark change is indicative of an upregulation of voiding activity and a lowering of bladder capacity. These results suggest a frequency-dependent, dual-modulatory effect of TNS on bladder function, a finding not previously captured computationally. The findings corroborate pre-clinical studies demonstrating an excitatory effect of low-frequency TNS on bladder function[17,18,19]. This dual-modulatory effect highlights the model's ability to capture not only the established effects of TNS but also an under-explored excitatory aspect. However, the mechanism behind this modulation remains unclear.

To address this question, we examined the impact severing specific tibial projections had on the circuit wide effects of TNS during low frequency (1Hz), and high frequency (10Hz) stimulation. One-way ANOVAs revealed a significant effect of connective state on pelvic efferent activity in both low-frequency ($F_{(5,24)} = 135.04, p < 0.001$) and high-frequency ($F_{(5,24)} = 49.85, p < 0.001$) conditions. Bonferonni adjusted post-hoc testing confirmed that severing all brainstem-targeting projections (i.e., both PAG and PMC) eliminated the low-frequency effect. In this severed condition, pelvic activity returned to baseline, and did not significantly differ from unstimulated levels ($p = 0.38$, see fig. 2B(ii)). Moreover, where brainstem projections remained intact (causing an excitation in pelvic output), severing spinal projections had no significant influence on this excited state of pelvic activity ($p = 0.50$, see fig. 2B(ii)). Taken together, these results indicate that brainstem targeting projections likely mediate the low-frequency excitatory outcome of TNS. However, they do not pinpoint which specific part of the brainstem (PAG or PMC) is essential to the effect, as inhibition of either module was sufficient to induce a significant excitation of the system from baseline ($p < 0.001$ in both cases).

In contrast, during high-frequency stimulation every possible connective state drove a significant decrease in pelvic activity from baseline ($p < 0.001$ in all cases, see fig. 2B(iii)). While it is clear tibial projections are required in some form to induce an inhibitory effect, the specific targets that mediate the void-inhibition cannot be determined.

This model for the first time provides a computational insight into TNS, supplementing the hypothesised mechanism of action derived experimentally[13] with circuit level evidence. Specifically, the present work strengthens the possibility that the tibial nerve impacts efferent activity through action on solely the afferent arm of the micturition circuit. It also explains the likely role of the brainstem in mediating a dual excitatory/inhibitory effect of TNS.

We characterise the role of brainstem as a filter. The inhibitory feedback mechanisms within the PAG and PMC (see fig. 1C labels 1-4) allow the modules to act as a set of high-pass filters connected in series, preventing efferent void signalling until a sufficient afferent firing rate is reached. Low-frequency TNS may induce an excitatory effect by inhibiting these feedback mechanisms, reducing the threshold of the filters, thereby allowing a smaller afferent signal to trigger void-promoting efferent activity. Conversely, the strong inhibition induced by high-frequency TNS may be sufficient to suppress the production of any void-promoting efferent activity, despite the reduced threshold of the filters. Nevertheless, it is unclear if this high-frequency inhibition occurs at the level of the spine, silencing afferent activity before it reaches the filters (fig. 1C, label 5), or at the level of the brainstem, silencing communication between the modules that allows for the production of void-promoting efferent activity (fig. 1C, labels 2-4) or the efferent activity itself (fig. 1C, label 1).

This hypothesis is supported by previous modelling work[15] which indicated that altering the strength of tonic inhibition in the PMC could modulate bladder capacity. As such, it is reasonable to suggest that TNS induces a similar effect in the PAG via inactivation of the tonic inhibitory neurons that dampen PAG-PMC transmission (fig 1C, labels 3/4). However, the present findings reveal that inhibiting either region causes a similar system-level increase in voiding behaviour. As such, it cannot be said whether PAG or PMC would mediate a change in bladder activity *in vivo*. Further research is necessary to answer this question, and to examine which combination of projections is required to produce the high frequency inhibitory effect observed. Nevertheless, the proposed model provides computational evidence for a role of the brainstem in an excitatory effect of TNS and potentially high-frequency inhibition of non-nociceptive bladder activity.

These findings have clinical implications for the treatment of non-obstructive urinary retention. At present few non-invasive interventions for the condition exist[20]. While existing studies using 20Hz TNS show modest promise[21,22], our modelling work suggests their limited efficacy may be due to the use of sub-optimal stimulation frequencies. Therefore, further research will examine the feasibility of low-frequency TNS as a treatment option for urinary retention.

Our computational model focused on non-nociceptive bladder activity and, therefore, the reported effects of TNS cannot generalise to nociceptive conditions, as irritation may alter the bladder's response to the intervention[13]. This is less concerning for the application of TNS in the treatment of urinary retention, however, which typically involves sensory dysfunction rather than nociception[23,24]. Nevertheless, the model offers valuable insight into the usefulness of TNS as a therapy for urinary retention. Furthermore, it provides a strong foundation for future research efforts which may elucidate the precise neural

mechanisms underlying the complex effects of TNS on bladder function in both healthy and diseased states.

Code availability

The custom code used for analysis in this study is available upon reasonable request from the corresponding author.

Acknowledgements

This project is funded in part by the University of Edinburgh and the Engineering and Physical Sciences Research Council (EPSRC) grant number EP/W031493/1.

Author contributions statement

A.M.T conceived the study, constructed the model, and analysed the results; M.J. processed and prepared the bladder data used to fit the model and run simulations in the present study; M.J. and A.E. generated the animal bladder data; A.M.T and M.J. produced the figures used in the publication; K.N. provided research guidance and advice; All authors reviewed the manuscript.

Competing interests

The authors declare no competing interests.

References

[1] Clare J. Fowler, Derek Griffiths, and William C. De Groat. "The neural control of micturition". In: *Nature reviews. Neuroscience* 9.6 (June 2008), p. 453. ISSN: 1471003X. DOI: 10.1038/NRN2401.

[2] William C. de Groat, Derek Griffiths, and Naoki Yoshimura. "Neural Control of the Lower Urinary Tract". In: *Comprehensive Physiology* 5.1 (Jan. 2015), pp. 327–396. ISSN: 20404603. DOI: 10.1002/CPHY.C130056.

[3] Daniel Jaskowak et al. "Mathematical modeling of the lower urinary tract: A review". In: *Neurourology and Urodynamics* 41.6 (Aug. 2022), pp. 1305–1315. ISSN: 1520-6777. DOI: 10.1002/NAU.24995.

[4] William C. de Groat and Changfeng Tai. "Impact of Bioelectronic Medicine on the Neural Regulation of Pelvic Visceral Function". In: *Bioelectronic Medicine* 2.1 (June 2015), pp. 25–36. ISSN: 23328886. DOI: 10.15424/BIOELECTRONMED.2015.00003.

[5] Tomonori Yamanishi et al. "Neuromodulation for the Treatment of Lower Urinary Tract Symptoms". In: *LUTS: Lower Urinary Tract Symptoms* 7.3 (Sept. 2015), pp. 121–132. ISSN: 1757-5672. DOI: 10.1111/LUTS.12087.

[6] Mahipal Choudhary, Ron van Mastrigt, and Els van Asselt. "Inhibitory effects of tibial nerve stimulation on bladder neurophysiology in rats". In: *SpringerPlus* 5.1 (Dec. 2016), pp. 1–8. ISSN: 21931801. DOI: 10.1186/S40064-016-1687-6.

[7] Thomas W. Fuller et al. "Sex difference in the contribution of GABAB receptors to tibial neuromodulation of bladder overactivity in cats". In: *American Journal of Physiology - Regulatory Integrative and Comparative Physiology* 312.3 (Mar. 2017), R292–R300. ISSN: 15221490. DOI: 10.1152/AJPREGU.00401.2016.

[8] Todd Yecies et al. "Spinal interneuronal mechanisms underlying pudendal and tibial neuromodulation of bladder function in cats". In: *Experimental Neurology* 308 (Oct. 2018), pp. 100–110. ISSN: 0014-4886. DOI: 10.1016/J.EXPNEUROL.2018.06.015.

[9] Zhaocun Zhang et al. "Role of μ, κ, and δ Opioid Receptors in Tibial Inhibition of Bladder Overactivity in Cats". In: *Journal of Pharmacology and Experimental Therapeutics* 355.2 (Nov. 2015), pp. 228–234. ISSN: 0022-3565. DOI: 10.1124/JPET.115.226845.

[10] Yosuke Matsuta et al. "Contribution of opioid and metabotropic glutamate receptor mechanisms to inhibition of bladder overactivity by tibial nerve stimulation". In: *American Journal of Physiology - Regulatory Integrative and Comparative Physiology* 305.2 (July 2013), pp. 126–133. ISSN: 03636119. DOI: 10.1152/AJPREGU.00572.2012.

[11] Matthew C. Ferroni et al. "Role of the brain stem in tibial inhibition of the micturition reflex in cats". In: *American Journal of Physiology - Renal Physiology* 309.3 (Aug. 2015), F242–F250. ISSN: 15221466. DOI: 10.1152/AJPRENAL.00135.2015.

[12] Changfeng Tai et al. “Differential role of opioid receptors in tibial nerve inhibition of nociceptive and nonnociceptive bladder reflexes in cats”. In: *American Journal of Physiology - Renal Physiology* 302.9 (2012), pp. 1090–1097. ISSN: 15221466. DOI: 10.1152/AJPRENAL.00609.2011.

[13] Xunhua Li, Xing Li, and Limin Liao. “Mechanism of Action of Tibial Nerve Stimulation in the Treatment of Lower Urinary Tract Dysfunction”. In: *Neuromodulation: Technology at the Neural Interface* 27.2 (Feb. 2024), pp. 256–266. ISSN: 1094-7159. DOI: 10.1016/J.NEUROM.2023.03.017.

[14] Joanne Booth et al. “The effectiveness of transcutaneous tibial nerve stimulation (TTNS) for adults with overactive bladder syndrome: A systematic review”. In: *Neurourology and Urodynamics* 37.2 (Feb. 2018), pp. 528–541. ISSN: 1520-6777. DOI: 10.1002/NAU.23351.

[15] W. C. De Groat and C. Wickens. “Organization of the neural switching circuitry underlying reflex micturition”. In: *Acta Physiologica* 207.1 (Jan. 2013), pp. 66–84. ISSN: 1748-1716. DOI: 10.1111/APHA.12014.

[16] Milad Jabbari and Abbas Erfanian. “Estimation of Bladder Pressure and Volume from the Neural Activity of Lumbosacral Dorsal Horn Using a Long-Short-Term-Memory-based Deep Neural Network”. In: *Scientific Reports 2019 9:1* 9.1 (Dec. 2019), pp. 1–15. ISSN: 2045-2322. DOI: 10.1038/s41598-019-54144-8.

[17] Shun Li et al. “Prolonged nonobstructive urinary retention induced by tibial nerve stimulation in cats”. In: *American Journal of Physiology - Regulatory Integrative and Comparative Physiology* 318.2 (Feb. 2020), R428–R434. ISSN: 15221490. DOI: 10.1152/AJPREGU.00277.2019.

[18] Zainab Moazzam, Austin R. Duke, and Paul B. Yoo. “Inhibition and Excitation of Bladder Function by Tibial Nerve Stimulation Using a Wirelessly Powered Implant: An Acute Study in Anesthetized Cats”. In: *The Journal of Urology* 196.3 (Sept. 2016), pp. 926–933. ISSN: 15273792. DOI: 10.1016/J.JURO.2016.04.077.

[19] Katherine Theisen et al. “Frequency Dependent Tibial Neuromodulation of Bladder Underactivity and Overactivity in Cats”. In: *Neuromodulation: Technology at the Neural Interface* 21.7 (Oct. 2018), pp. 700–706. ISSN: 1094-7159. DOI: 10.1111/NER.12792.

[20] Wesley M. White et al. “Sacral Nerve Stimulation for Treatment of Refractory Urinary Retention: Long-Term Efficacy and Durability”. In: *Urology* 71.1 (Jan. 2008), pp. 71–74. ISSN: 0090-4295. DOI: 10.1016/J.UROLOGY.2007.08.034.

[21] Rosa L. Coolen et al. “Transcutaneous Electrical Nerve Stimulation and Percutaneous Tibial Nerve Stimulation to Treat Idiopathic Nonobstructive Urinary Retention: A Systematic Review”. In: *European Urology Focus* 7.5 (Sept. 2021), pp. 1184–1194. ISSN: 2405-4569. DOI: 10.1016/J.EUF.2020.09.019.

[22] Gabriele Gaziev et al. “Percutaneous tibial nerve stimulation (PTNS) efficacy in the treatment of lower urinary tract dysfunctions: A systematic review”. In: *BMC Urology* 13.1 (Nov. 2013), pp. 1–11. ISSN: 14712490. DOI: 10.1186/1471-2490-13-61.

[23] Jacek K. Szymański, Aneta Słabuszewska-Jóźwiak, and Grzegorz Jakiel. “Fowler’s Syndrome—The Cause of Urinary Retention in Young Women, Often Forgotten, but Significant and Challenging to Treat”. In: *International Journal of Environmental Research and Public Health 2021, Vol. 18, Page 3310* 18.6 (Mar. 2021), p. 3310. ISSN: 1660-4601. DOI: 10.3390/IJERPH18063310.

[24] Stephen W. Leslie, Prashanth Rawla, and Joseph M. Dougherty. “Female Urinary Retention”. In: *StatPearls*. Treasure Island, (FL): StatPearls, May 2023. URL: https://www.ncbi.nlm.nih.gov/books/NBK538497/.

Methods

Model Topology

The simulated network was composed of a set of interconnected neuronal units each comprising 100 individuals neurons modelled in terms of conductance, or poisson point processes that generated simulated action potentials (see Neuronal Model). The topology of the model was adapted from previous work which simulated reflex voiding[15]. The circuit remained broadly unmodified with the exception of additional projections representing the tibial nerve, and the method used to model bladder function. Tibial nerve projections targeted: second order sensory afferents (via classical inhibitory synapses), and all neuronal units within the PAG and PMC (via opioidergic inhibitory synapses). Specific projections could be severed by disconnecting these synaptic junctions, meaning that while the neurons were still modelled their activity had no impact on post-synaptic targets.

Bladder Model

Rather than deploy a full biophysical model of the organ, the study represented the bladder as a mathematical vector containing the internal bladder pressure ($P_B(t)$) and volume ($V_B(t)$) for any given timestep (t) of the simulation. The sample rate of the vector was 50Hz, with each step (t) representing a 20ms increment. The bladder data used to do so was obtained from previously published work[16] (see Animal Model Surgery and Preparation). Given the nature of the model organ, the simulation of urine-flow sensitive urethral afferents was not required.

Simulation Pipeline

Each run of the simulation began by supplying bladder data to simulate specific lower urinary tract activity. From this information the initial firing rate of the primary pressure sensitive afferents ($F(P_B(t))$) was calculated, and the equations governing the neurons/synapses within the circuit integrated. The instantaneous firing rate of any target neurons was calculated and saved, and the simulation incremented to the next timestep where the process was repeated. The simulation was halted when the model reached the end of the supplied bladder data.

Animal Model Surgery and Preparation

To run the simulated model, we utilised real bladder pressure and neural data from a previously published work[16]. During the constant infusion of the bladder, simultaneous recording of neural signals from the spinal cord was conducted. To measure bladder pressure and volume, a catheter was inserted into the bladder wall from the dome area and secured using a purse-string suture, in such a way that one head of catheter was connected to pressure transducer and second one to the infusion pump. To measure the voided volume, a digital scale was positioned under the rat model, and the residual volume was calculated through the difference between the infusion volume and the voided amount. A single-channel recording was performed using epoxylite-insulated tungsten electrodes with resistance of 300-500 $k\Omega$ and shank diameter of 75 μm (FHC Inc., Bowdin, ME USA). To facilitate three-dimensional control of electrode tip, a micro-manipulator (SM-15, Narishige Group Product, Japan) was utilised providing possibility of locating electrode in best anatomical position. To reduce the effect of noise on the recorded signals, a custom-made Faraday cage was employed to envelop the entire experimental setup.

Neuronal Model

The model was built using the Brian2 package for python[25]. The relationship between pelvic afferent firing rate and bladder pressure was calculated according to an empirically derived relationship determined previously[26] where the firing rate of the primary bladder afferent at each moment ($F(P_B(t))$) was defined as:

$$F(P_B(t)) = \begin{cases} -3\times10^{-8}P_B(t)^5 + 1\times10^{-5}P_B(t)^4 - 1.5\times10^{-3}P_B(t)^3 + 7.9\times10^{-2}P_B(t)^2 - 0.6P_B(t) & F(P_B(t)) \geq 0Hz \\ \\ 0Hz & F(P_B(t)) < 0Hz \end{cases} \tag{1}$$

All neuronal units, with the exception of primary bladder afferents, and the tibial nerve were simulated using a Conductance-Based Adaptive Exponential Integrate-and-Fire (CAdEx) model[27] modified to include opioidergic inhibition. Through the inclusion of an additional input current (I_{ap}) neurons could be made tonically active where required. This was particularly important in the simulation of the PAG and PMC, where inhibitory feedback mechanisms reliant on tonic activity were present.

The tibial nerve and primary bladder afferents were simulated as poisson point processes which generated simulated neuronal spikes at a pre-specified rate. Doing so allowed the firing rate of the pelvic afferent to be set according to the

aforementioned mathematical relation, and the firing rate of the tibial nerve to be clamped to a specific value (representing external stimulation of the nerve).

Each *unit* within the network was composed of 100 simulated neurons connected via random synapses (where no autapses were permitted) to introduce noise to the system.

Membrane potential (v) was defined as

$$C_m \frac{dv}{dt} = g_L(E_L - v) + g_L \Delta_t \exp\left(\frac{v - v_{th}}{\Delta_t}\right) + g_A(E_A - v) + I_{ap} + I_{syn} \tag{2}$$

where C_m was the membrane capacitance; g_L the leakage current & E_L its associated reversal potential; g_A was the adaption current and E_A its reversal potential; I_{ap} the input to tonically firing neurons; and I_{syn} the input from synaptic connections. Also included were terms governing the action potential (v_{th} and Δ_t). Like the original model, g_A was defined as:

$$\tau_A \frac{dg_A}{dt} = \frac{\bar{g_A}}{1 + \exp\left(\frac{v_A - v}{\Delta_A}\right)} - g_A \tag{3}$$

where the rate of change of the current was determined by a rate constant (τ_A), the subthreshold adaption parameters (v_A and Δ_A), and the maximum subthreshold adaption conductance ($\bar{g_A}$). The model also included a post-spike reset mechanism, which too remained unchanged.

$$\text{if } v \geq 0mV \text{ then } \begin{cases} v & \mapsto v_R \\ g_A & \mapsto g_A + \delta g_A. \end{cases} \tag{4}$$

Upon spiking the membrane potential was reset to its resting state (v_R), and the adaption current incremented (δg_A). The purpose of the adaption current was to allow for the modelling of spike-frequency adaption. Tonically active neurons did not display spike-frequency adaption to ensure their activity remained consistent.

Synaptic Model

Synapses were modelled in terms of conductance using established formulae[28], modified to include opioidergic transmission. The magnitude of the synaptic current (I_{syn}) was defined as:

$$I_{syn} = g_{ex}(E_{ex} - v) + g_{in}(E_{in} - v) + g_{op}(E_{op} - v) \tag{5}$$

where $g_{ex/in}$ represents the conductance of classical excitatory/inhibitory currents, and $E_{ex/in}$ their reversal potentials; and g_{op}/E_{op} representing the action of opioid currents. Each of the modelled synaptic conductances decayed exponentially according to

$$\frac{dg_{ex/in/op}}{dt} = \frac{-g_{ex/in/op}}{\tau_{ex/in/op}}. \tag{6}$$

Synaptic strength was weighted, such that upon presynaptic spiking, the postsynaptic conductance of either excitatory, inhibitory, or opioidergic currents was incremented according to:

$$g_{ex/in/op} \mapsto g_{ex/in/op} + w\delta g_{ex/in/op} \tag{7}$$

where w represents the weighting factor, and $\delta g_{ex/in/op}$ the baseline increase in conductance in response to a presynaptic spike. The weights of all synaptic connections were determined by parameter fitting and constrained within a specific range to allow controlled plasticity within the network.

Model Optimisation

Bayesian optimisation was used to fit the parameters of the model[29]. To do so, the activity of second order sensory afferents was extracted, downsampled to 10Hz, and smoothed (1st order Butterworth Filter, 1Hz cutoff frequency). This data was compared to the ground-truth neural data associated with the input bladder data (see Animal Model Surgery and Preparation) producing a normalised root mean square error (NRMSE) value representing the difference between the simulated activity and expected activity. The algorithm fit the weights and parameters of the model such that the NRMSE was minimised (acquisition function - Gaussian hedging, acquisition optimiser - LMBFGS, N_{calls} = 200). After running the algorithm, specific weights were manually tweaked to further optimise the efferent activity of the model, ensuring it was accurate to typical bladder behaviour.

Bayesian optimisation of model weights and parameters considerably improved the accuracy of simulated afferent activity, bringing it closer to ground truth neural data ($NRMSE_{baseline}$=3.367; $NRMSE_{optimised}$=1.454). While subsequent manual tweaking did improve the efferent behaviour of the model it did lead to a slight increase in NRMSE suggesting it did so at the cost of afferent accuracy ($NRMSE_{fitted} = 1.599$). Despite the minor decrease in global function fit, this methodology nevertheless improved the efferent behaviour of the model and allowed the simulation to better capture the peaking pattern of neuronal firing rates in the afferent arm of the circuit (see supplementary fig. 1) providing an accurate foundation for analysing the effects of neuromodulation. Notably, the optimisation algorithm reached its minimum NRMSE plateau in a reasonable number of calls suggesting the global function minimum was true (see supplementary fig. 2).

Although these results are positive, some technical limitations should be considered. The model did not capture all peaks in the firing rate, and did not replicate the physiological noise present in the data. While noise ommission might affect the model's ability to capture very specific network behaviours, the current level of accuracy is sufficient to serve as a foundation for exploring the modulatory mechanism of TNS.

Tibial Nerve Stimulation Analysis

To analyse the impact of tibial modulation on the system, set bladder data was supplied to the simulation. The firing rate of the pelvic efferent (which typically drives detrusor contraction) was analysed as the primary measure of bladder activity. The area under the curve (AUC) of the smoothed firing rate (1st order Butterworth filter, with a 1Hz cutoff) was calculated under a range of frequencies of tibial neuromodulation (0 - 20Hz, in 1Hz increments). Five simulation runs were conducted at each frequency, and 0Hz stimulation data was taken as the baseline measure of activity.

To analyse the effect of specific tibial projections, the same procedure was performed at baseline (0Hz) and under low (1Hz), and high (10Hz) frequency tibial stimulation. In each case, tibial projections to the region of interest were severed by preventing the formation of synaptic connections.

Model Parameters

Where possible these were matched to the parameters described in the original papers describing the neuronal and synaptic models[27,28]. Key parameters that were fit included the current mediating tonic activity (I_{ap}), the magnitude of excitatory and inhibitory conductance ($g_{ex/in/op}$), and the upper magnitude of spike-frequency adaption ($\bar{g}_A$). See supplementary table 1 for the parameters used in the simulation.

Methods References

[15] W. C. De Groat and C. Wickens. "Organization of the neural switching circuitry underlying reflex micturition". In: *Acta Physiologica* 207.1 (Jan. 2013), pp. 66–84. ISSN: 1748-1716. DOI: 10.1111/APHA.12014.

[16] Milad Jabbari and Abbas Erfanian. "Estimation of Bladder Pressure and Volume from the Neural Activity of Lumbosacral Dorsal Horn Using a Long-Short-Term-Memory-based Deep Neural Network". In: *Scientific Reports 2019 9:1* 9.1 (Dec. 2019), pp. 1–15. ISSN: 2045-2322. DOI: 10.1038/s41598-019-54144-8.

[25] Marcel Stimberg, Romain Brette, and Dan F.M. Goodman. "Brian 2, an intuitive and efficient neural simulator". In: *eLife* 8 (Aug. 2019). ISSN: 2050084X. DOI: 10.7554/ELIFE.47314.

[26] Meredith J. McGee and Warren M. Grill. "Modeling the spinal pudendo-vesical reflex for bladder control by pudendal afferent stimulation". In: *Journal of Computational Neuroscience* 40.3 (June 2016), pp. 283–296. ISSN: 15736873. DOI: 10.1007/s10827-016-0597-5.

[27] Tomasz Górski, Damien Depannemaecker, and Alain Destexhe. "Conductance-Based Adaptive Exponential Integrate-and-Fire Model". In: *Neural Computation* 33.1 (Jan. 2021), pp. 41–66. ISSN: 0899-7667. DOI: 10.1162/NECO{_}A{_}01342.

[28] T. P. Vogels et al. "Inhibitory plasticity balances excitation and inhibition in sensory pathways and memory networks". In: *Science* 334.6062 (Dec. 2011), pp. 1569–1573. ISSN: 10959203. DOI: 10.1126/SCIENCE.1211095.

[29] Mike Diessner et al. “Investigating Bayesian optimization for expensive-to-evaluate black box functions: Application in fluid dynamics”. In: *Frontiers in Applied Mathematics and Statistics* 8 (Dec. 2022), p. 1076296. ISSN: 22974687. DOI: 10.3389/FAMS.2022.1076296.

Figures & Tables

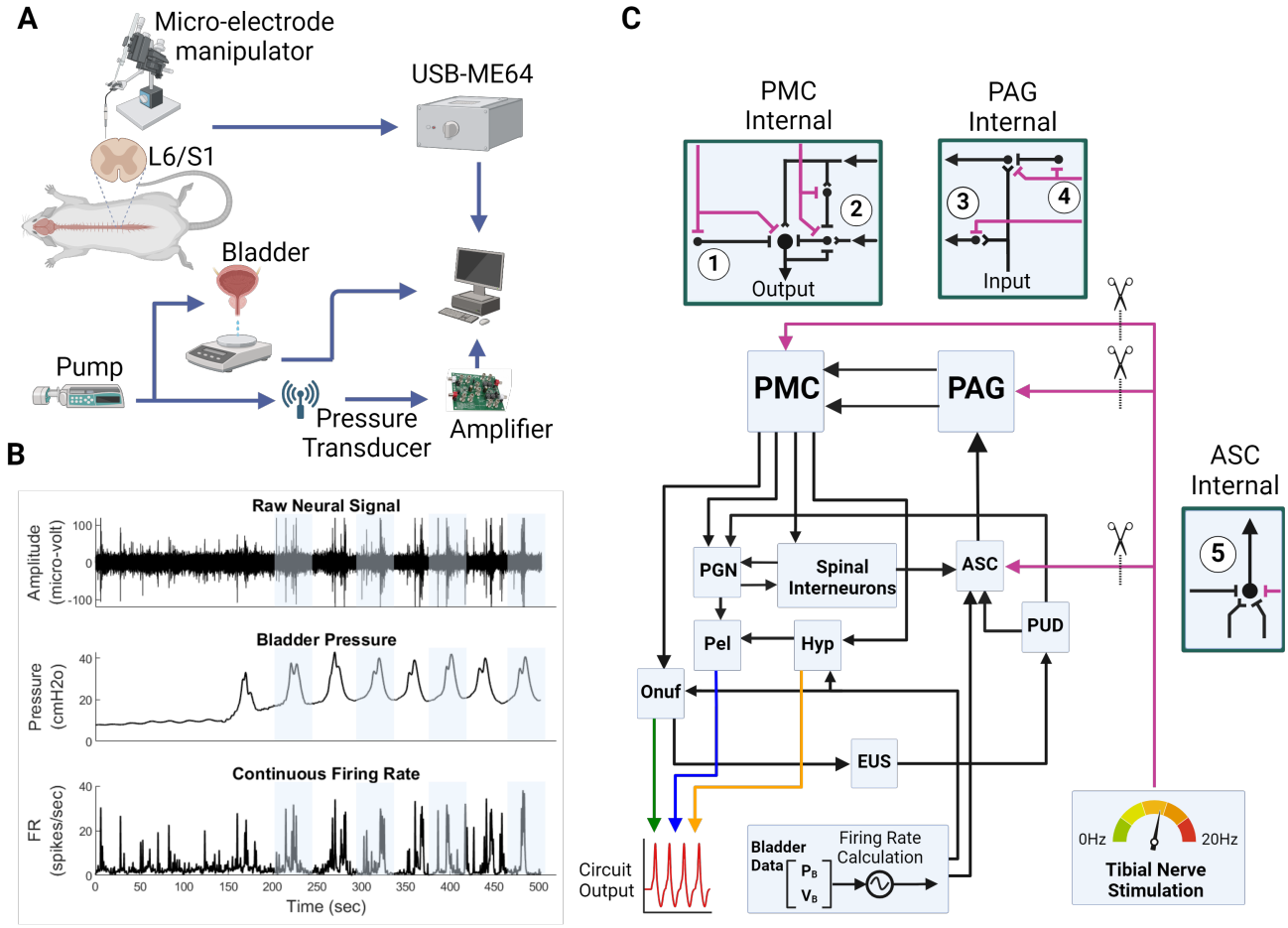

Figure 1. Methodological approach used to simulate Tibial Nerve Stimulation (TNS). A. Experimental setup and recording site used to obtain bladder data and associated afferent neural signal. **B.** Bandpass-filtered raw neural signal (top trace), corresponding bladder pressure (middle trace), and smoothed continuous neural firing rate (1st order Butterworth filter with a 1Hz cutoff frequency, bottom trace) obtained from the experimental setup. **C.** Block diagram of the simulated neuronal circuit. The model used experimentally obtained bladder pressure/volume data as input to generate corresponding circuit level activity. Tibial input used to modulate the circuit shown in purple. The key efferent projections used as the main output measure for the simulation represented in blue (Pelvic nerve), green (Pudendal nerve) and orange (Hypogastric nerve). PMC: Pontine Micturition Centre, PAG: Periaquaductal Grey, PGN: Preganglionic Bladder Neurons, ASC: Ascending Interneurons, PUD: Pudendal Afferent, Onuf: Onuf's Nucleus, EUS: External Urethral Sphincter, Pel: Pelvic Efferent, Hyp: Hypogastric Efferent. Scissors represent possible severed projections. Labels 1 - 5 represent key regions of tibial modulation using opioidergic (1 - 4) or classical (5) inhibitory mechanisms.

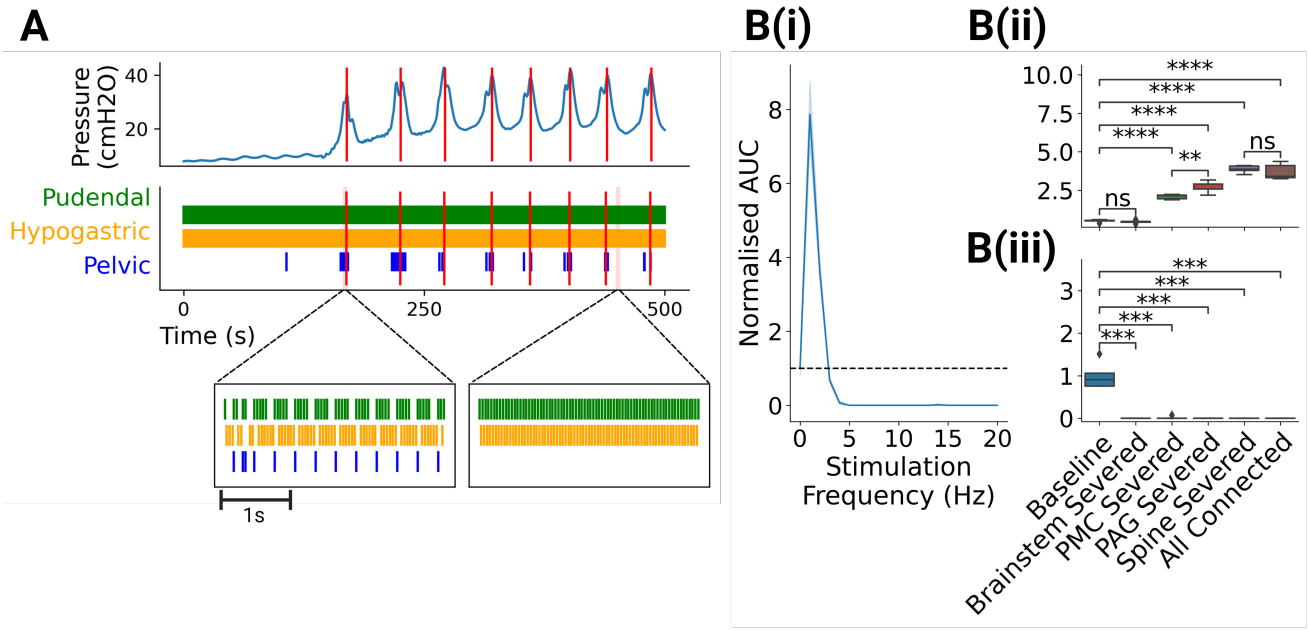

Figure 2. Behaviour of Normal and Tibial-Modulated Circuit Activity A. Simulated circuit response for given bladder data input. Shown is the example bladder data used (top trace) and a raster plot of the activity in the three major efferent projections mediating bladder function (bottom plot). Red lines represent voiding events in the bladder data. Blowout boxes show efferent activity during voiding (left) and storage (right). **B(i).** Frequency dependent effect of tibial neuromodulation on pelvic (void promoting) efferent activity. Efferent firing rate was smoothed (1st order Butterworth filter, 1Hz cutoff frequency) and the AUC for the trace calculated to give a measure of the magnitude of the void signal for a given set of bladder data. AUC values were normalised against the activity of the circuit under zero tibial neuromodulation (baseline behaviour, dashed line). Error bars = $\pm 1SE$, $n_{runs} = 5$ for each tested frequency. **B(ii/iii)**. Effects of severing specific tibial projections on circuit behaviour. Shown are the effects on low frequency (1Hz, B(ii)) and high frequency (10Hz, B(iii)) modulation relative to baseline (no tibial modulation). All plots report normalised Pelvic AUC, ns: $p > 0.05$, **:$p < 0.01$, ***:$p < 0.001$, ****:$p < 0.0001$. Multiple comparisons were Bonferonni adjusted, $n_{runs} = 5$ for each condition.

Supplementary Materials

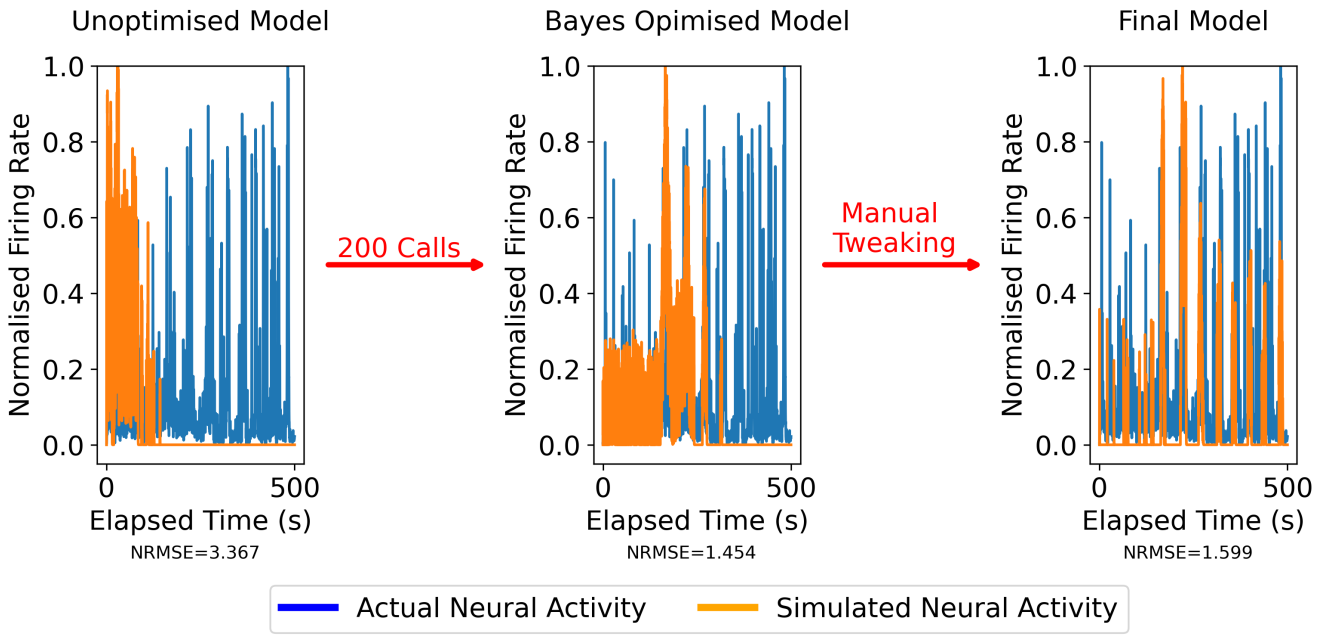

Supplementary Figure 1. Model Performance During Fitting Process. Shown is the overlap between ground truth (blue) and simulated (orange) afferent neural activity for a subset of bladder pressure data. Model performance is shown in a random unoptimised state (left), after 200 rounds of Bayesian optimisation (centre), and after final manual optimisation of model weights (right). The magnitude of the overlap between simulated and ground truth data at each stage shown as Normalised Root Mean Square Error (NRMSE). Smoothed firing rate (1st order butterworth filter, 1Hz cutoff frequency) was normalised against the maximum recorded value in each dataset.

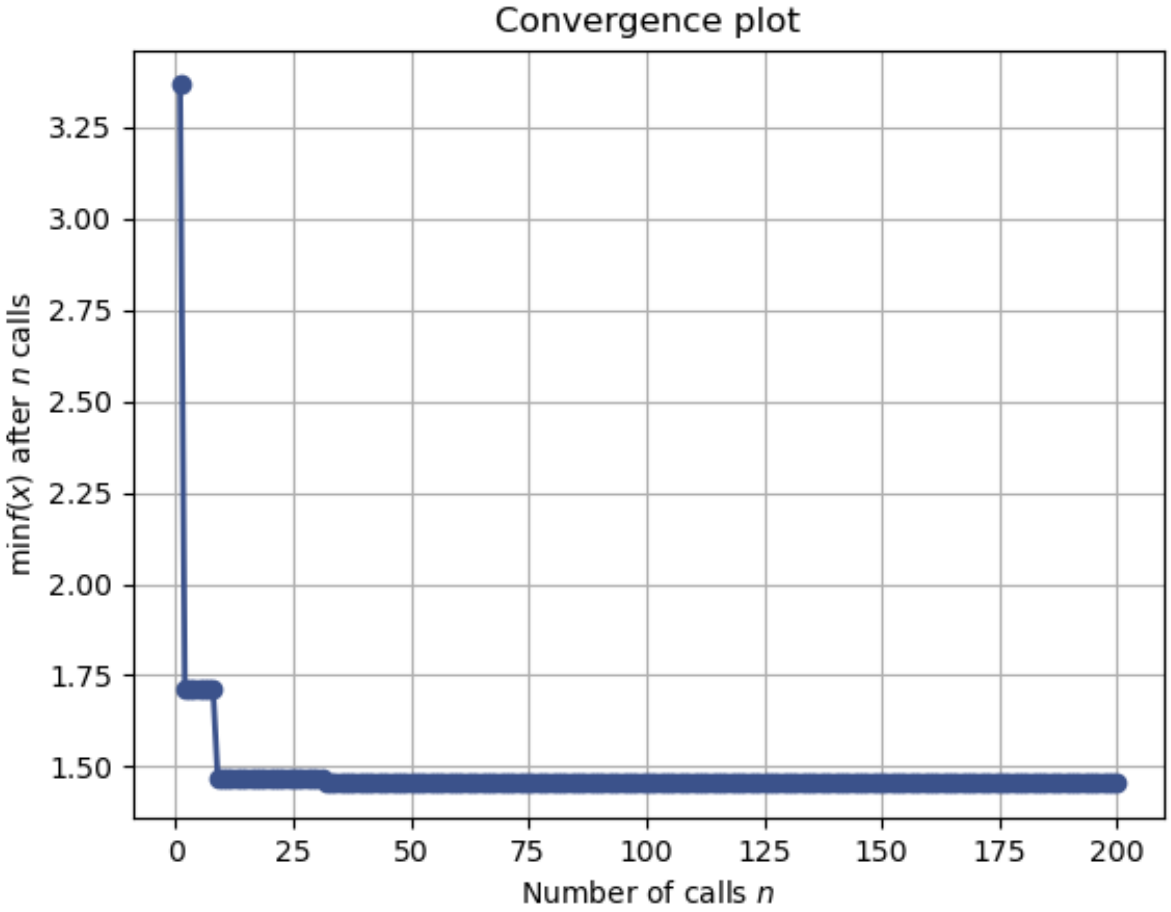

Supplementary Figure 2. Bayesian Optimisation Convergence Plot. Shown is a convergence plot detailing the Normalised Root Mean Square Error (NRMSE) of the ground truth vs. simulated afferent activity data at each phase of the optimisation process.

Parameter	Value
Membrane Capacitance (C_m)	200pF
Tonic Activity Input Current (I_{ap})*	175.35pA
Leak Current Reversal Potential (E_L)	-60mV
Leak Current Reversal Potential - Tonically Active Neurons (E_{LTonic})	-70mV
Reversal Potential of Excitatory Current (E_{ex})	0mV
Reversal Potential of Inhibitory Current (E_{in})	-80mV
Reversal Potential of Opioidergic Current (E_{op})	-80mV
Reversal Potential of Adaption Current (E_A)	-70mV
Leak Current Increment (g_L)	10nS
Excitatory Current Increment (g_{ex})*	0.51nS
Inhibitory Current Increment (g_{in})*	1.40nS
Opioidergic Current Increment (δg_{op})*	1.5nS
Adaption Current Increment (δg_A)	1nS
Adaption Current Increment - Tonically Active Neurons (δg_{ATonic})	0nS
Maximum Adaption Current ($\bar{g}_A$)*	10.17nS
Maximum Adaption Current - Tonically Active Neurons ($\bar{g}_{ATonic}$)	2nS
Activation Threshold for Adaption Current (V_A)	-50mV
Activation Threshold for Adaption Current - Tonically Active Neurons (v_{ATonic})	-45mV
Adaption Current Slope (Δ_A)	5mV
Post-Spike Reset Potential (v_R)	-55mV
Spike Threshold (v_{th})	-50mV
Spike Initiation Slope (Δ_t)	10mV
Refractory Period (Δ_{tRef})	5ms
Opioidergic Current Decay Constant (τ_{op})	10ms
Excitatory Current Decay Constant (τ_{ex})	5ms
Inhibitory Current Decay Constant (τ_{in})	10ms
Neuroplastic Decay Constant (τ_{STDP})	20ms
Adaption Current Decay Constant - Tonically Active Neurons (τ_{ATonic})	40ms
Adaption Current Decay Constant (τ_A)	200ms
Synaptic Learning Rate	5×10^{-3}
Target Postsynaptic Firing Rate (p_o)	1Hz

Supplementary Table 1. Final model parameters. Where possible parameters were matched to the original specifications of the neuronal/synaptic model. Parameters that were altered by the model fitting process are marked as *.